Research on the Connection Performance of SMA Pipe Coupling for Sports Equipment

Xudong Yang, Fan Gu, Yuyu Zhang, and Yuhan Jiang

Abstract Based on the constitutive relation of shape memory alloy (SMA) proposed by Auricchio and Taylor, a numerical simulation study was carried out on the connection performance and the functional failure mechanism of SMA pipe coupling, and the effect of interference magnitude, the wall thickness of SMA connector on the stress distribution and tensile strength was investigated. The simulation result shows that with the increase of interference magnitude, the Mises stress of the SMA pipe coupling increases accordingly, as well as the ultimate pullout load increases. With the increase of the wall thickness of SMA connector, the Mises stress of the SMA connector decreases, whereas the Mises stress of connected steel pipe increases. Furthermore, it is suggested that the gradual internal chamfer should be machined at both ends of SMA connector to alleviate the stress concentration. To improve the connection performance and the tensile strength of SMA pipe coupling, it should take into consideration concurrently to the increase of the wall thickness and the length of the SMA connector to avoid the yield failure of steel pipe.

Keywords Shape memory alloy · Pipe coupling · Connection performance · Constitutive relation · Numerical simulation

1 Introduction

In the early 1940s, Olander discovered the shape memory effect in Au-Cd alloy for the first time, after that scholars successively discovered the shape memory effect in Cu-Sn alloy and Cu–Zn alloy. At present, with the advantaged characteristics of shape memory effect, super-elasticity, fatigue resistance, corrosion resistance, high damping, and high resistance, the shape memory alloy (SMA) has been widely

X. Yang
Sports Department, Shenyang Jianzhu University, Shenyang, China

F. Gu (✉) · Y. Zhang · Y. Jiang
School of Civil Engineering, Shenyang Jianzhu University, Shenyang, China
e-mail: guzhaozheng@yeah.net

Y. Li et al. (eds.), *Advances in Simulation and Process Modelling*,
Advances in Intelligent Systems and Computing 1305,
https://doi.org/10.1007/978-981-33-4575-1_8

Fig. 1 Application of titanium alloy in sports products

applied in the fields of aerospace, civil engineering, machinery, medicine, bioengineering, sports equipment, and so on [1–5]. According to statistics, 16–20% of the total titanium alloy is used in sports and leisure products, becoming the third largest application market of titanium alloy, such as golf clubs, tennis rackets, badminton bats, fencing masks, sprinting shoe nails, climbing tools, diving suits, fishing tackle, tent poles, racing parts, and so on, as shown in Fig. 1.

Some sports products make use of titanium alloy on its characteristics of high strength, lightweight, and super-elastic properties, such as titanium alloy golf clubs with lightweight can improve golfer's hitting ratio and hitting distance significantly, the titanium alloy handle applied on tennis rackets and badminton bats can increase the instantaneous inertia force and striking force effectively, and racing bike parts produced by titanium alloy can reduce the weight and wind resistance concurrently. On the other hand, some sports products make use of titanium alloy on the shape memory effect. For example, the mechanical vibration of automobile gearbox occurs at elevated temperature due to the different thermal expansion coefficient of each gear, SMA gasket on the driving shaft can provide elastic recovery force constantly with the increase of temperature, which can improve the fastening force and reduce running noise. For another example, the traditional automotive oil pipe joint usually adopts welding technology, and the corrosion protection layer on the inner surface near the welding seam is easy to fail at elevated temperature. As an alternative product, SMA automotive pipe coupling can effectively avoid corrosion leakage, and the shape memory effect guarantees it good connection performance at elevated temperature.

At present, scholars mainly concentrate on the perspective of metallography and microstructure and have carried out the studies of SMA on the evolution of microstructure, phase transformation, magnetization behavior, shape memory behavior, and its influence factors such as annealing time and transformation temperatures. [6–11]. With the characteristic of shape memory effect and recovery driving force, Ni–Ti SMA and Fe–Mn–Si SMA are beginning to be used in pipe coupling of sports automobile and airplane [12]. Comparatively, from the point of macroscopic mechanical, the researches on the connection performance of SMA pipe coupling is insufficient. Zhang et al. [13, 14] and Gu et al. [15] carried out experimental and numerical researches on the connection performance of SMA pipe coupling and proposed the influence of wall thickness and inner diameter on the radial compressive stress of SMA pipe coupling. Jin et al. [16] studied the influence of predeformation temperature on the recovery performance of Ni–Ti–Nb SMA pipe joint. Chen et al. [17] conducted numerical research on the relationship of Ni–Ti–Nb SMA pipe

Table 1 Geometric parameters of SMA pipe coupling model

SMA pipe connector	Outer diameter/mm	Inner diameter /mm	Wall thickness/mm	Inner diameter before expanding/mm	Prestrain/%
	41.2	37.1	2.0	1.5	1.5
Connected steel pipe	Outer diameter/mm	Inner diameter /mm	Wall thickness/mm	Fit clearance/mm	Interference magnitude /mm
	36.78	34.78	1.0	0.160	0.115

coupling between radial stress, tension force, and temperature. Due to the complexity of the constitutive relation of SMA, the research on the connection performance of SMA pipe coupling was mainly conducted by experiment. In this paper, based on the constitutive relation of SMA proposed by Auricchio and Taylor [18], the numerical research was investigated on the stress distribution and failure mechanism of SMA pipe coupling, in order to provide the theoretical reference to the optimization design of SMA connector.

2 Numerical Model of SMA Pipe Coupling

According to the geometric parameters in Table 1, the numerical model of SMA pipe coupling was developed, and the axisymmetric solid element CAX4R was adopted for representing SMA connector and connected steel pipe. Due to the axisymmetric characteristics of the SMA pipe coupling, the generatrix model was adopted to establish. According to the constitutive relation of SMA proposed by Auricchio and Taylor, the SMA material parameters were evaluated as shown in Table 2 and Fig. 2, where E_M and E_A are the elastic modulus of martensite and austenite, respectively. At the reference temperature, σ_{TL}^{S} and σ_{TL}^{E} are the starting critical stress and the ending critical stress in the process of tensile loading, respectively, σ_{TU}^{S} and σ_{TU}^{E} are the starting critical stress and the ending critical stress in the process of unloading, respectively, and σ_{CL}^{S} is the starting critical stress in compressive loading process.

3 Connection Performance Analysis

3.1 Stress Distribution Analysis

When two steel pipes and SMA connector were assembled together, the SMA connector was heated to the predefined temperature of 600 °C. With the process of reverse martensitic transformation, SMA connector deforms to its original dimension

Table 2 Material parameters of SMA connector

Poisson's ratio	Elasticity modulus (GPa)	Critical stress of phase transformation (MPa)	Constant of phase transformation (MPa °C^{-1})	Strain of phase transformation	Reference temperature (°C)
0.33	$E_M = 55$ $E_A = 170$	$\sigma_{TL}^{S} = 520$	$\left(\frac{\delta\sigma}{\delta t}\right)_L = 8.0$ $\left(\frac{\delta\sigma}{\delta t}\right)_U = 13.8$	0.067	600
		$\sigma_{TL}^{E} = 750$			
		$\sigma_{TU}^{S} = 550$			
		$\sigma_{TU}^{E} = 200$			
		$\sigma_{CL}^{S} = 520$			

	Martensite's Young's Modulus	Martensite's Poisson's Ratio	Transformation Strain	Start of Transformation (Loading)	End of Transformation (Loading)	Start of Transformation (Unloading)	End of Transformation (Unloading)	Start of Transformation in Compression (Loading)	Reference Temperature	Loading	Unloading	Value of field variable that triggers shape setting
1	55000000000	0.33	0.067	520000000	750000000	550000000	200000000	520000000	600	8000000	13800000	0

Fig. 2 Setting in ABAQUS of the material parameters and hyper-elastic parameters of SMA

and makes two steel pipes connect together as a whole. The Mises stress distribution nephogram of SMA pipe coupling can be obtained, as shown in Fig. 3.

According to the symmetry of SMA pipe coupling model in axial direction, the semi-structure in axial direction was selected as analysis object, and the radial stress nephogram and the circumferential stress nephogram of SMA pipe coupling are shown in Fig. 4. It can be seen that the radial stress of SMA connector is distributed evenly along the axial direction and decreases gradually along the radial direction from inner surface to outside surface, and the radial stress of connected steel pipe is distributed evenly along the axial direction and increases gradually along the radial direction from inner surface to outside surface. The circumferential stress distributions of SMA connector and connected steel pipe are evenly both in axial direction and radial direction, and their absolute values vary within the range of [134.7, 146.5 MPa] and [275.8, 302.3 MPa], respectively. In addition, the stress concentration phenomenon occurs in the contact area near the ends of SMA connector, where the radial stress of interaction is about −25.2 MPa, and the absolute values of circumferential stress of SMA connector and connected steel pipe reach 146.5 and 302.3 MPa, respectively. As is known that SMA connector and connected steel pipe

Fig. 3 Mises stress distribution nephogram of SMA pipe coupling

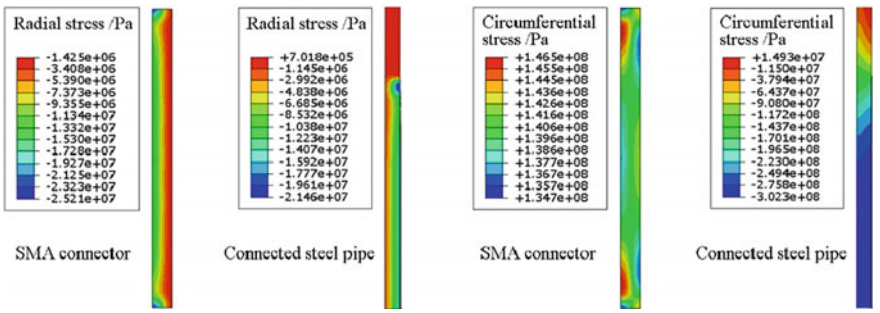

(a) The radial stress distribution (b) The circumferential stress distribution

Fig. 4 Stress nephogram of the semi-structure of SMA pipe coupling

are thin-walled circular tube structure, the absolute value of its circumferential stress is much greater than that of radial stress according to Lamè formula [19].

3.2 Connection Performance and Influence Factors

Pullout load was exerted on the end of steel pipes, the relation between load and displacement is as shown in Fig. 5, and the radial stress nephogram of SMA connector is as shown in Fig. 6. It can be seen that the axial displacement of SMA pipe coupling is proportional to the pullout load in the initial stage of axial tension, and there is no sliding occurrence between SMA connector and steel pipes, which means that the axial displacement of SMA pipe coupling is completely caused by elastic deformation. When the pullout load reaches the ultimate value, sliding between SMA connector and steel pipe occurs leading the axial displacement increases rapidly. With the increase of axial displacement, the friction area between SMA connector and steel pipes decreases gradually, leading to the decrease of pullout load.

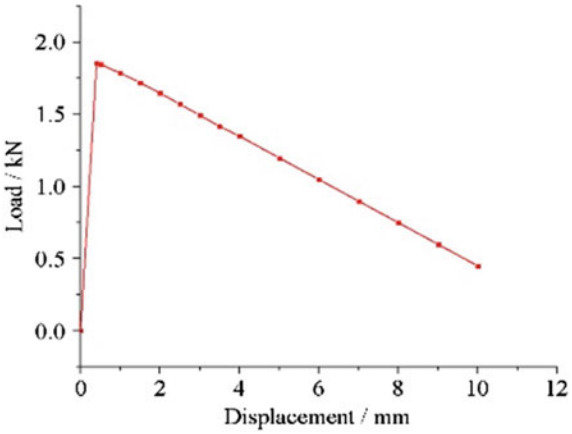

Fig. 5 Relation between load and displacement

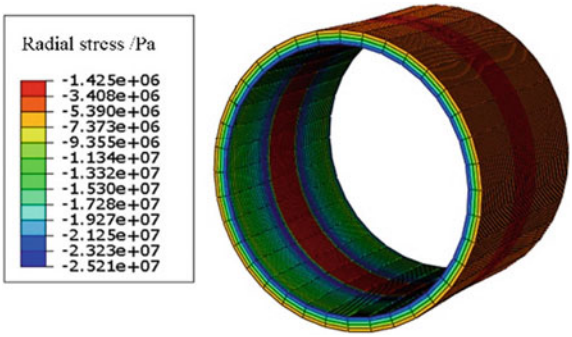

Fig. 6 Radial stress nephogram of connector

Five numerical models of SMA pipe coupling were developed with difference interference magnitude of 0.065, 0.115, 0.165, 0.215, and 0.265 mm, respectively, and other geometric parameters being the same as those in Table 1. With the difference interference magnitude, the stress nephogram of SMA pipe coupling could be gotten as shown in Fig. 7. It can be seen that the stress concentration occurs in the contact area near the ends of SMA connector. The absolute value of the radial stress at this location was extracted, and the relation between the maximum absolute value of radial stress and the interference magnitude could be obtained, as shown in Fig. 8. In addition, the relation between the ultimate pullout load and the interference magnitude could be investigated as shown in Fig. 9. It can be seen that with the increase of the interference magnitude, the maximum absolute value of radial stress and the ultimate pullout load increase accordingly.

Similarly, five SMA pipe coupling numerical models were established with difference wall thickness of SMA connector of 1, 2, 3, 4, and 5 mm, respectively, and the relation between the maximum absolute value of radial stress and the wall thickness of SMA connector, the relation between the ultimate pullout load and the wall thickness of SMA connector could be obtained as shown in Figs. 10 and 11. It can be seen that with the increase of the wall thickness of SMA connector, the maximum absolute value of radial stress and the ultimate pullout load increase accordingly, as soon as the circumferential stress of steel pipe increases whereas the circumferential stress of SMA connector decreases simultaneously.

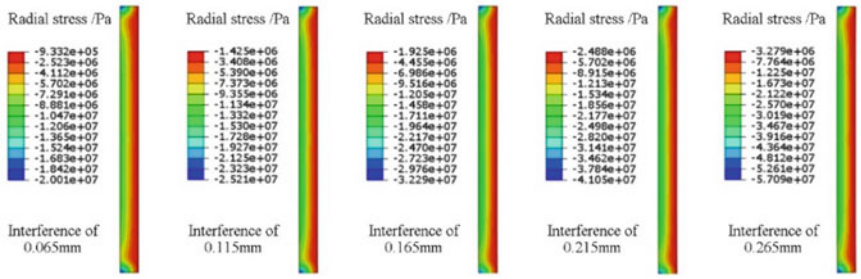

(a) Radial stress nephogram of SMA connector with different interference magnitude.

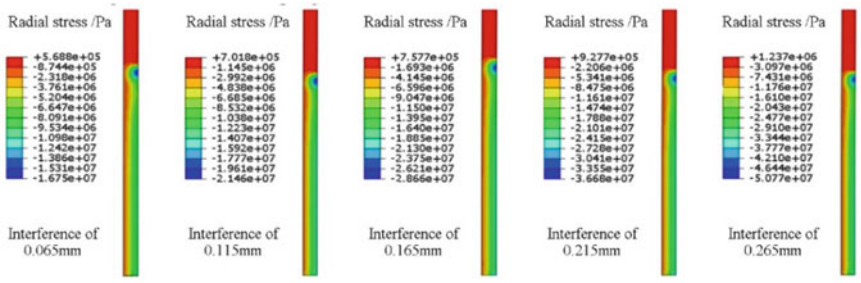

(b) Radial stress nephogram of steel pipe with different interference magnitude.

Fig. 7 Radial stress nephogram of SMA pipe coupling with different interference magnitude

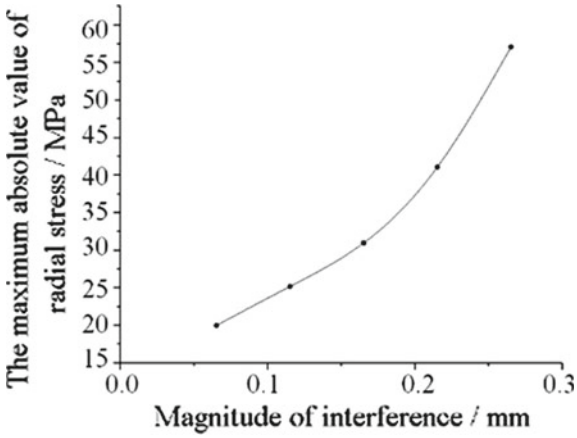

Fig. 8 Relation between the maximum value of radial stress and the interference magnitude

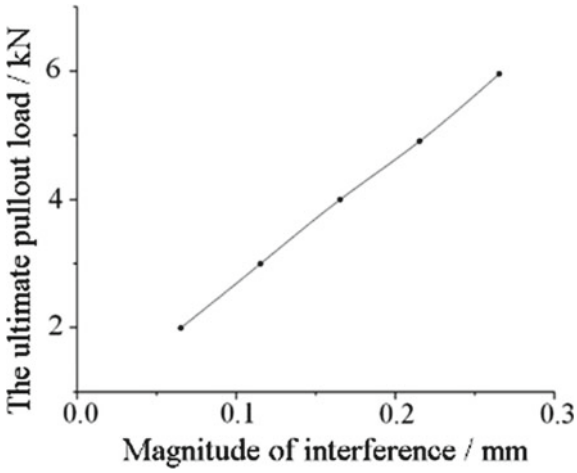

Fig. 9 Relation between the ultimate pullout load and the interference magnitude

4 Conclusions

Based on the constitutive relation of SMA proposed by Auricchio and Taylor, the numerical simulation research on the connection performance of SMA pipe coupling was carried out, and numerical simulation result shows the conclusions as follows.

1. The stress concentration phenomenon occurs in the contact area near the ends of SMA connector, and the gradual internal chamfer should be machined at both ends of SMA connector to alleviate the stress concentration.

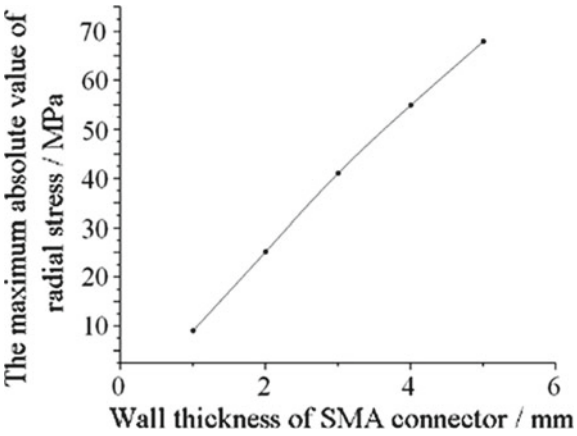

Fig. 10 Relation between the max. value of radial stress and the wall thickness of connector

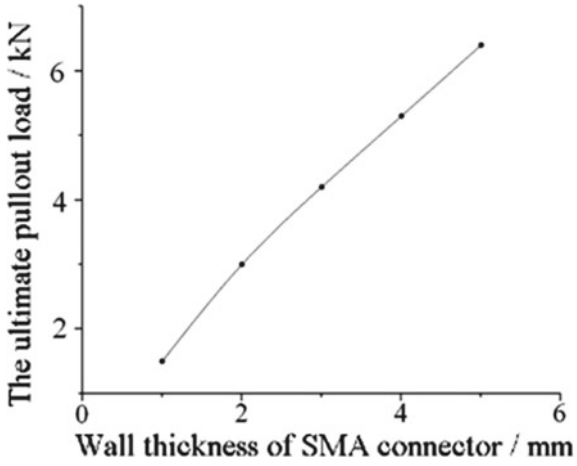

Fig. 11 Relation between the ultimate pullout load and the wall thickness of connector

2. Under the action of pullout load, in the initial stage, the axial displacement of SMA pipe coupling caused by elastic deformation is proportional to the pullout load.
3. When the pullout load reaches the ultimate value, the axial displacement of SMA pipe coupling increase rapidly caused by frictional sliding between SMA connector and steel pipes. With the increase of the axial displacement of SMA pipe coupling, the friction area decreases gradually, leading to the decrease of pullout load accordingly.
4. The increase of the wall thickness of SMA connector is equivalent to the increase of the relative stiffness of SMA connector, which will lead to the decrease of the

Mises stress of SMA connector and the increase of the Mises stress of steel pipe. Therefore, in the process of the design of SMA pipe coupling, to improve the tensile strength of SMA pipe coupling, it should take into consideration concurrently to the increase of the wall thickness and the length of SMA connector to avoid the yield failure of steel pipe.

Acknowledgements This research work is supported by Scientific Research Project of Liaoning Science and Technology Department (Project Codes: 2019-ZD-0297) and Scientific Research Project of Shenyang Jianzhu University (Project Codes: 2017007).

References

1. Khan, M.I., Pequegnat, A., Zhou, Y.N.: Multiple memory shape memory alloys. Adv. Eng. Mater. **15**(5), 386–393 (2013)
2. Lee, S.H., Kim, S.W.: Improved position control of shape memory alloy actuator using the self-sensing model. Sens. Actuators Phys. **297**(1), 64–72 (2019)
3. Ren, H.M., Peng, G.S.: Research on application of SMA in structure strengthening and rehabilitation. Struct. Eng. **34**(6), 175–180 (2018) (in Chinese)
4. Niskanen, A.J., Laitinen, I.: Design and simulation of a magnetic shape memory (MSM) alloy energy harvester. Adv. Sci. Technol. **78**(1), 58–62 (2013)
5. Ren, Y.S., Tian, J.S., Liu, Y.L., Du, C.G.: Nonlinear deformation, thermal buckling and vibration of SMA fiber composite beams. J. Shandong Univ. Sci. Technol. (Nat. Sci.) **38**(1), 99–110 (2019) (in Chinese)
6. He, Z.R., Liu, M.Q.: Effects of annealing and deforming temperature on microstructure and deformation characteristics of Ti-Ni-V shape memory alloy. Mater. Sci. Eng., B **177**(12), 986–991 (2012)
7. Velmurugan, C., Senthikumar, V., Kamala, P.S.: Microstructure and corrosion behavior of NiTi shape memory alloys sintered in the SPS process. Int. J. Miner. Metall. Mater. **26**(10), 1311–1321 (2019)
8. Peng, H.B., Yong, L.Q., Wang, S.L., Wen, Y.H.: Role of annealing in improving shape memory effect of as-cast Fe-Mn-Si-Cr-Ni shape memory alloys. Metall. Mater. Trans. A **50**(1), 3070–3079 (2019)
9. Zhang, J., Ma, Y.H., Wu, R.L., Wang, J.M.: Shape memory effect of dual-phase NiMnGaTb ferromagnetic shape memory alloys. J. Iron. Steel Res. Int. **26**(1), 321–328 (2019)
10. Haidar, M.A., Saud, S.N., Hamzah, E.: Microstructure, mechanical properties, and shape memory effect of annealed Cu-Al-Ni-*x*Co shape memory alloys. Metall. Microstruct. Anal. **7**(1), 57–64 (2018)
11. Shuwadi, M.F., Saud, S.N., Hamzah, E.: Deformation influences on microstructure, mechanical properties, and shape memory behavior of Cu-Al-Ni-*x*Ti shape memory alloys. Metall. Microstruct. Anal. **8**(1), 406–414 (2019)
12. Gu, F., Zhang, L., Wang, W., Zhang, Y.Y.: Review of shape memory alloy pipeline coupling. Constr. Budg. **260**(12), 30–37 (2017) (in Chinese)
13. Zhang, H.B., Wang, J., Jin, W., Yang, R.: Coupling force simulation of TiNiFe shape memory alloy pipe-coupling. Chin. J. Nonferrous Meta. **20**(Special 1), 510–513 (2010) (in Chinese)
14. Zhang, H.B., Jin, W., Yang, R.: 3D finite element simulation of pull-out force of TiNiFe shape memory pipe coupling with inner convex. ACTA Metall. Sinca. **48**(12), 1520–1524 (2012) (in Chinese)
15. Gu, F., Song, J.R, Hou, Y.X., Zhang, L.: Research on connection performance of shape-memory-alloy pipe joint. J. Shenyang Jianzhu Univ. (Nat. Sci.) **36**(2), 307–313 (2020) (in Chinese)

16. Jin, L.L., Lu, S.Q., Li, G.F., Wang, K.R., Liu, J.W.: Effect of pre-deformed temperature on recovery property of $Ni_{47}Ti_{44}Nb_9$ alloy Φ8mm pipe joint. J. Nanchang HangKong Univ. (Nat. Sci.) **26**(4), 71–77 (2012) (in Chinese)
17. Chen, Q., Wang, K.L., Lu, S.Q., Li, G.F.: Numerical simulation analysis of Φ10mm NiTiNb shape memory alloy pipe-coupling. Hot Working Technol. **46**(2), 74–77 (2017) (in Chinese)
18. Auricchio, F., Taylor, R.L.: Shape-memory alloys: modelling and numerical simulations of the finite-strain superelastic behavior. Comput. Methods Appl. Mech. Eng. **143**(1), 175–194 (1997)
19. Xu, Z.L.: Elasticity. High Education Press, Beijing (2016)